



Syntheses, third-order optical nonlinearity and DFT studies on benzoylferrocene derivatives



Jianhong Jia, Yanhong Cui, Liang Han, Weijian Sheng, Yujin Li, Jianrong Gao*

College of Chemical Engineering and Materials Science, Zhejiang University of Technology, Hangzhou 310032, PR China

ARTICLE INFO

Article history:

Received 20 October 2013

Received in revised form

23 December 2013

Accepted 3 January 2014

Available online 13 January 2014

Keywords:

Benzoylferrocene derivatives

Nonlinear optics

DFWM technique

The third-order NLO

Functional dyes

Density Functional Theory

ABSTRACT

A series of benzoylferrocene derivatives were synthesized and their third-order nonlinear optical (NLO) properties were evaluated in N,N-dimethyl-formamide at 800 nm using femtosecond degenerate four-wave mixing. The third-order NLO susceptibilities of synthesized compounds were $3.065\text{--}7.859 \times 10^{-13}$ esu, with the response times in 49–70 fs. The second-order hyperpolarizabilities of the molecules of the compounds were $1.018\text{--}2.611 \times 10^{-31}$ esu. The Density Functional Theory was used to calculate these benzoylferrocene derivatives. The theoretical study showed that the third-order NLO properties were increased with the increasing electron-withdrawing ability, which is accordance with the decreasing energy gap between the highest occupied and the lowest unoccupied molecular orbital. With the increasing of electron-withdrawing ability, the transferred charge to the substituent was increased and the affection on the electronic reallocate was increased. The experiment and theoretical results showed that the benzoylferrocene derivatives had potential nonlinear optical applications.

Crown Copyright © 2014 Published by Elsevier Ltd. All rights reserved.

1. Introduction

Design and synthesis of the excellent performance of the three order nonlinear optical (NLO) materials is a hot research topic in recent years [1]. Organic materials had been investigated as alternatives to inorganic species due to their low cost, fast and large nonlinear response over a broad frequency range, inherent synthetic flexibility, low dielectric constant, high optical-damage threshold, and intrinsic tailorability [2,3]. Nonlinear optical response of organic materials comes from the molecular polarizability of nonlocalized π -electron under the light field, which is different from inorganic materials. Because the movement of nonlocalized π -electron is easy and not affected by lattice vibrations, the NLO response of organic materials are stronger and faster than that of inorganic materials [4]. To date, many kinds of organic NLO materials have been synthesized, such as D–A push–pull structure of azo compounds [5,6], squaric acid [7], heterocyclic compounds [8,9], tetrathiafulvalene derivatives [10], schiff base complex [11], metal phthalocyanine compounds [12], and ferrocene derivatives [13]. Among them, metal complexes with potential NLO

properties, good thermal and photochemical stability, and redox switching abilities have caused considerable interests.

Ferrocene, with its unique electrical, magnetic, optical, redox, and crystal properties, as well as its high thermal and chemical stability, is a very useful building block in the construction of various functional materials and has been used in numerous medicinal and bioorganometallic chemistry applications [14–16]. In this context, we have been involved in the study of NLO properties of ferrocene derivatives. We had previously reported that ferrocene, as an electron donor and/or an acceptor was an excellent building block for the construction of organic NLO materials [17–21]. These studies had focused on the important role of ferrocene substituents enhancing third-order NLO properties of such materials. In addition, most process for synthesis of benzoylferrocene derivatives require extremely low temperature ($-78\text{ }^{\circ}\text{C}$) [22], strong corrosive reagent (triflic acid) [23], or abnormal reagent [24]. In the present work we found a simple and efficient method for the synthesis of benzoylferrocene derivatives (Fig. 1). The third-order NLO properties of these materials had been measured and compared with the data calculated by the Density Functional Theory (DFT) of quantum chemistry. The NLO properties were illustrated well with the energy of the highest occupied molecular orbital (HOMO), the energy of the lowest unoccupied molecular orbital (LUMO), the HOMO and LUMO gap (E_{gap}), the natural charge, and MOs. This is the first study on the NLO properties for

* Corresponding author.

E-mail address: zjutgjr@163.com (J. Gao).

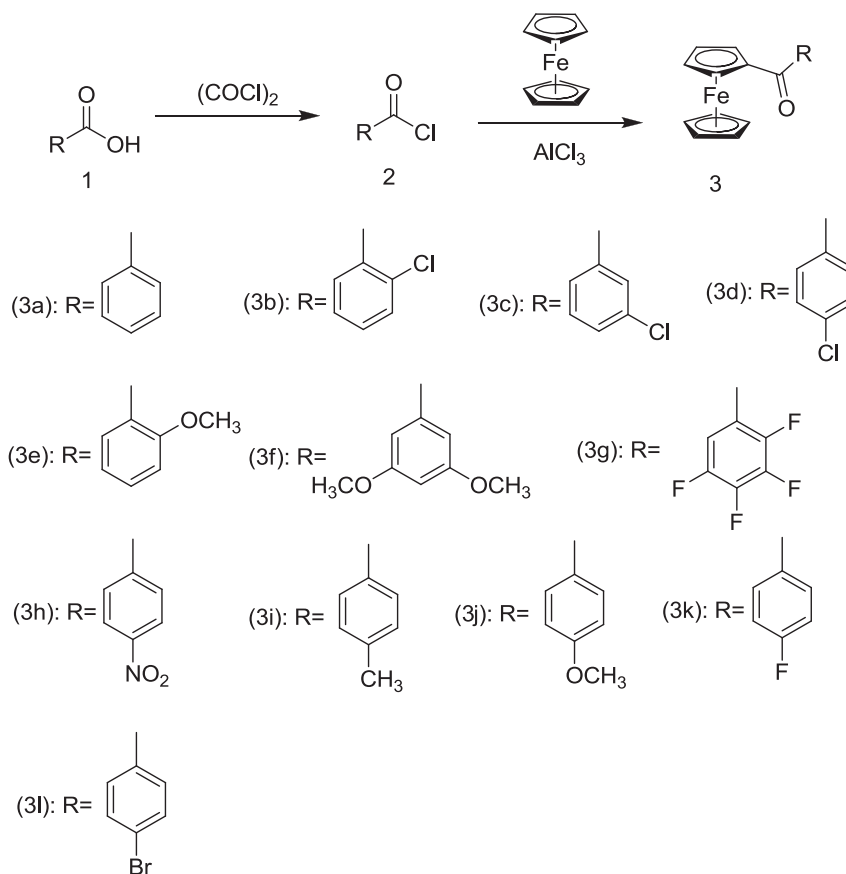


Fig. 1. Synthetic routes of benzoylferrocene derivatives.

benzoylferrocene derivatives by experiments combined with quantum chemistry.

2. Experimental section

2.1. Materials

Unless otherwise stated, starting materials were used as purchased without further purification. The dimethylformamide (DMF) was distilled from CaH_2 .

2.2. Instruments

The ^1H nuclear magnetic-resonance (^1H NMR) spectra were obtained on a Varian XL-200 spectrometer. Ultraviolet–visible (UV–vis) spectra were recorded on a Shimadzu UV-2550 UV–visible spectrophotometer using a quartz cuvette with a 1 cm path length. Low-resolution MS was obtained using EI ionizations. Melting points were measured with micro melting point apparatus.

2.3. Synthesis

2.3.1. General procedure for syntheses of benzoylferrocene derivatives

A mixture of 10.0 mmol benzoic acid derivatives 1, 50.0 mL chloroform, 1 to 2 drops of DMF as catalyst, and oxalyl chloride (1.90 g, 15.0 mmol) was stirred at room temperature for 3.0–4.0 h. The solvent and excess oxalyl chloride were removed by rotary evaporation to produce crude benzoyl chloride derivatives 2.

Ferrocene (1.86 g, 10.0 mmol) was combined with chloroform (50.0 mL) and stirred at 0–5 °C. Afterward, the above crude benzoyl chloride derivatives was dissolved in 15.0 mL chloroform and added slowly. Anhydrous aluminum chloride (8.0 g, 60.0 mmol) was added in batches. The mixture was warmed to room temperature for at least 1.0 h. The reaction was quenched with the ice water (100 mL), and then the mixture was shaken, standing and demixed. The organic layer was evaporated to dryness by rotary evaporation after washing with alkali and water. The residue was purified by chromatography on silica gel to afford benzoylferrocene derivatives 3.

2.3.2. Benzoylferrocene (3a)

Red powder; yield 64.9%, m.p. 109–110 °C. ^1H NMR (500 MHz, CDCl_3) δ = 7.92–7.90 (m, 2H, Ar–H), 7.57–7.56 (m, 1H, Ar–H), 7.50–7.48 (m, 2H, Ar–H), 4.93–4.92 (t, J = 2.0 Hz, 2H, Cp–H), 4.61–4.60 (t, J = 2.0 Hz, 2H, Cp–H), 4.23 (s, 5H, Cp–H), MS (EI), m/z : 291.0 (M^+).

2.3.3. 2-Chlorobenzoylferrocene (3b)

Red powder; yield 67.7%, m.p. 99–100 °C. ^1H NMR (500 MHz, CDCl_3) δ = 7.53–7.51 (d, J = 7.5 Hz, 1H, Ar–H), 7.48–7.46 (d, J = 8.0 Hz, 1H, Ar–H), 7.43–7.41 (t, J = 6.5 Hz, 1H, Ar–H), 7.39–7.36 (t, J = 7.0 Hz, 1H, Ar–H), 4.775 (s, 2H, Cp–H), 4.626 (s, 2H, Cp–H), 4.308 (s, 5H, Cp–H), MS (EI), m/z : 325.5 (M^+).

2.3.4. 3-Chlorobenzoylferrocene (3c)

Red powder; yield 52.4%, m.p. 102–103 °C. ^1H NMR (500 MHz, CDCl_3) δ = 7.73 (s, 1H, Ar–H), 7.65–7.63 (d, J = 7.5 Hz, 1H, Ar–H),

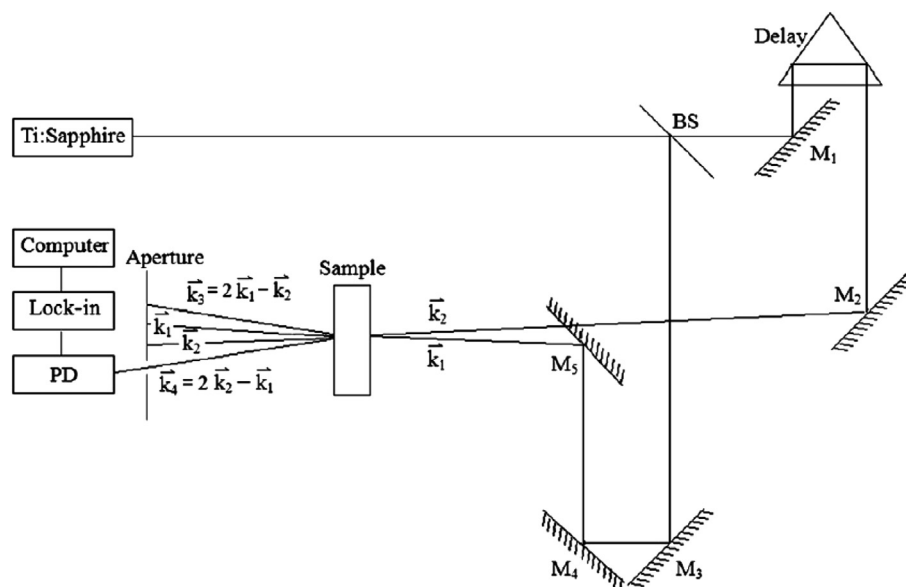


Fig. 2. Optical path of DFWM.

7.52–7.48 (t, $J = 9.5$ Hz, 1H, Ar–H), 7.39–7.33 (t, $J = 7.0$ Hz, 1H, Ar–H), 4.80 (s, 2H, Cp–H), 4.63 (s, 2H, Cp–H), 4.31 (s, 5H, Cp–H), MS (EI), m/z : 325.5 (M^+).

2.3.5. 4-Chlorobenzoylferrocene (**3d**)

Red powder; yield 41.9%, m.p. 122–123 °C. $^1\text{H NMR}$ (500 MHz, CDCl_3) $\delta = 7.87$ –7.58 (d, $J = 8.5$ Hz, 2H, Ar–H), 7.46–7.44 (d, $J = 8.5$ Hz, 2H, Ar–H), 4.88 (t, $J = 2.0$ Hz, 2H, Cp–H), 4.61–4.60 (t, $J = 1.5$ Hz, 2H, Cp–H), 4.202 (s, 5H, Cp–H), MS (EI), m/z : 325.5 (M^+).

2.3.6. 2-Methoxybenzoylferrocene (**3e**)

Red powder; yield 61.2%, m.p. 138–139 °C. $^1\text{H NMR}$ (500 MHz, CDCl_3) $\delta = 7.45$ –7.42 (m, 2H, Ar–H), 7.03–7.00 (m, 2H, Ar–H), 4.76 (t, $J = 2.0$ Hz, 2H, Cp–H), 4.55–4.54 (t, $J = 2.0$ Hz, 2H, Cp–H), 4.237 (s, 5H, Cp–H), 3.85 (s, 3H, OCH_3), MS (EI), m/z : 321.0 (M^+).

2.3.7. 3,5-Dimethoxybenzoylferrocene (**3f**)

Red powder; yield 18.3%, m.p. 84–85 °C. $^1\text{H NMR}$ (500 MHz, CDCl_3) $\delta = 7.07$ –7.06 (d, $J = 2.5$ Hz, 2H, Ar–H), 6.66–6.65 (t, $J = 2.0$ Hz, 1H, Ar–H), 4.95–4.94 (t, $J = 2.0$ Hz, 2H, Cp–H), 4.61–4.60 (t, $J = 2.0$ Hz, 2H, Cp–H), 4.237 (s, 5H, Cp–H), 3.875 (s, 6H, OCH_3), MS (EI), m/z : 351.0 (M^+).

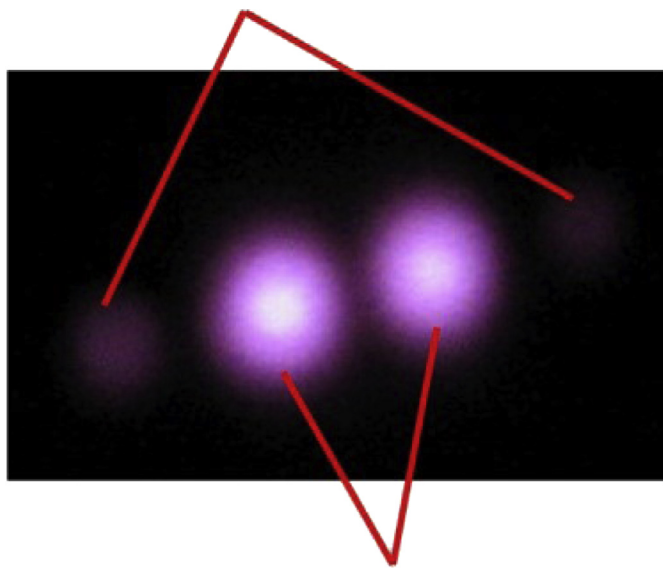
2.3.8. 2,3,4,5-Tetrafluorobenzoylferrocene (**3g**)

Red powder; yield 21.0%, m.p. 81–83 °C. $^1\text{H NMR}$ (500 MHz, CDCl_3) $\delta = 7.27$ –7.23 (m, 1H, Ar–H), 4.819 (s, 2H, Cp–H), 4.69–4.68 (t, $J = 2.0$ Hz, 2H, Cp–H), 4.254 (s, 5H, Cp–H), MS (EI), m/z : 363.0 (M^+).

2.3.9. 4-Nitrobenzoylferrocene (**3h**)

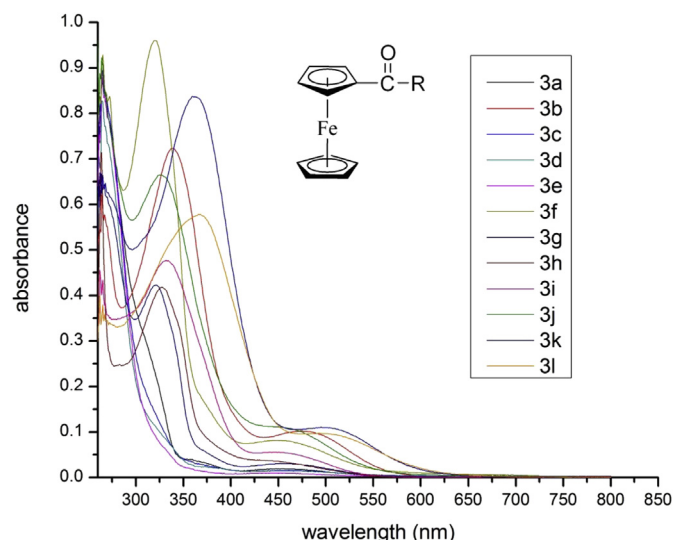
Red powder; yield 10.8%, m.p. 189–190 °C. $^1\text{H NMR}$ (500 MHz, CDCl_3) $\delta = 8.37$ –8.35 (m, 2H, Ar–H), 8.31–8.30 (m, 2H, Ar–H), 4.62–4.61 (t, $J = 4.0$ Hz, 2H, Cp–H), 4.292 (s, 5H, Cp–H), 4.07–4.06 (t, $J = 4.0$ Hz, 2H, Cp–H), MS (EI), m/z : 336.1 (M^+).

The phase-conjugated beam k3



The input beam k1 and k2

Fig. 3. The photo of phase-conjugated beam and input beam.

Fig. 4. The UV-vis spectrum of **3a**–**3l** in DMF.

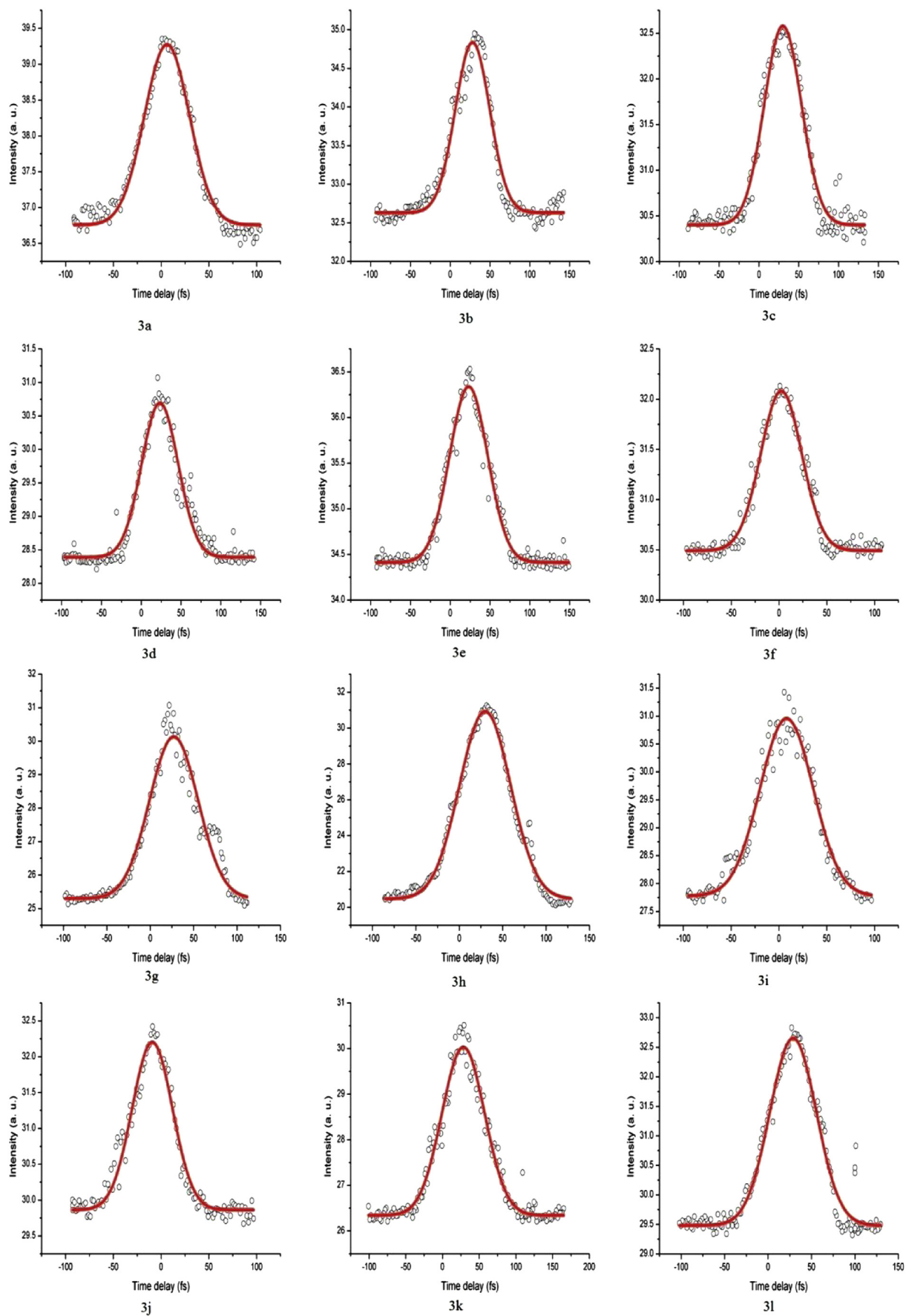


Fig. 5. DFWM signal versus delay time for 3a–3l in DMF solution.

Table 1
The values of $\chi^{(3)}$, γ , n_2 , and the respond times for **3a–3l**.

Compound <i>l</i>	<i>n</i>	$\chi^{(3)}$ (10^{-13} esu)	n_2 (10^{-12} esu)	γ (10^{-31} esu)	Response time τ (fs)	
3a	2.51656	1.4309	3.857	7.098	1.281	55.64
3b	2.2077	1.4300	3.608	6.648	1.199	51.15
3c	2.18091	1.4306	3.589	6.607	1.192	51.15
3d	2.30618	1.4303	3.689	6.795	1.226	54.20
3e	1.9277	1.4306	3.374	6.212	1.121	56.56
3f	1.59033	1.4307	3.065	5.642	1.018	50.84
3g	4.83337	1.4302	5.340	9.836	1.774	66.10
3h	10.46603	1.4303	7.859	14.475	2.611	69.42
3i	3.18123	1.4304	4.333	7.980	1.440	65.59
3j	2.34178	1.4310	3.721	6.847	1.236	49.71
3k	3.69335	1.4308	4.672	8.599	1.552	68.64
3l	3.17254	1.4303	4.327	7.969	1.437	63.03

2.3.10. 4-Methylbenzoylferrocene (**3i**)

Red powder; yield 42.1%, m.p. 129–130 °C. $^1\text{H NMR}$ (500 MHz, CDCl_3) δ = 8.17 (d, J = 8.0 Hz, 2H, Ar–H), 8.06 (d, J = 8.5 Hz, 2H, Ar–H), 4.80 (s, 2H, Cp–H), 4.54–4.42 (s, 2H, Cp–H), 4.24 (s, 5H, Cp–H), 2.36 (s, 3H, CH_3), MS (EI), m/z : 305.0 (M^+).

2.3.11. 4-Methoxybenzoylferrocene (**3j**)

Red powder; yield 63.8%, m.p. 125–126 °C. $^1\text{H NMR}$ (500 MHz, CDCl_3) δ = 8.25–8.08 (d, J = 8.0 Hz, 2H, Ar–H), 7.89 (d, J = 7.0 Hz,

2H, Ar–H), 4.77 (s, 2H, Cp–H), 4.45 (s, 2H, Cp–H), 4.23 (s, 5H, Cp–H), 3.86 (s, 3H, OCH_3), MS (EI), m/z : 321.0 (M^+).

2.3.12. 4-Fluorobenzoylferrocene (**3k**)

Red powder; yield 46.2%, m.p. 114–116 °C. $^1\text{H NMR}$ (500 MHz, CDCl_3) δ = 8.47–8.34 (d, J = 7.5 Hz, 2H, Ar–H), 7.16 (d, J = 7.0 Hz, 2H, Ar–H), 4.76–4.78 (m, 2H, Cp–H), 4.42 (s, 2H, Cp–H), 4.25 (s, 5H, Cp–H), MS (EI), m/z : 309.0 (M^+).

2.3.13. 4-Bromobenzoylferrocene (**3l**)

Red powder; yield 39.7%, m.p. 117–119 °C. $^1\text{H NMR}$ (500 MHz, CDCl_3) δ = 8.25–8.08 (d, J = 8.5 Hz, 2H, Ar–H), 7.89 (d, J = 7.5 Hz, 2H, Ar–H), 4.77 (s, 2H, Cp–H), 4.45 (s, 2H, Cp–H), 4.23 (s, 5H, Cp–H), MS (EI), m/z : 369.9 (M^+).

2.4. Nonlinear optical measurements

The third-order NLO properties were measured by DFWM with the 80 fs laser pulses (800 nm) generated by a Ti: sapphire laser with repetition rate of 1 kHz. The experiments were performed at 22 °C in DMF solutions using a 1 mm-thick quartz cell. As a reference, the optical nonlinearity of the standard sample (CS_2) was also observed.

The input beam was split into two beams (k_1 and k_2) of nearly equal energies using a beam splitter. The input beam, k_2 , passed

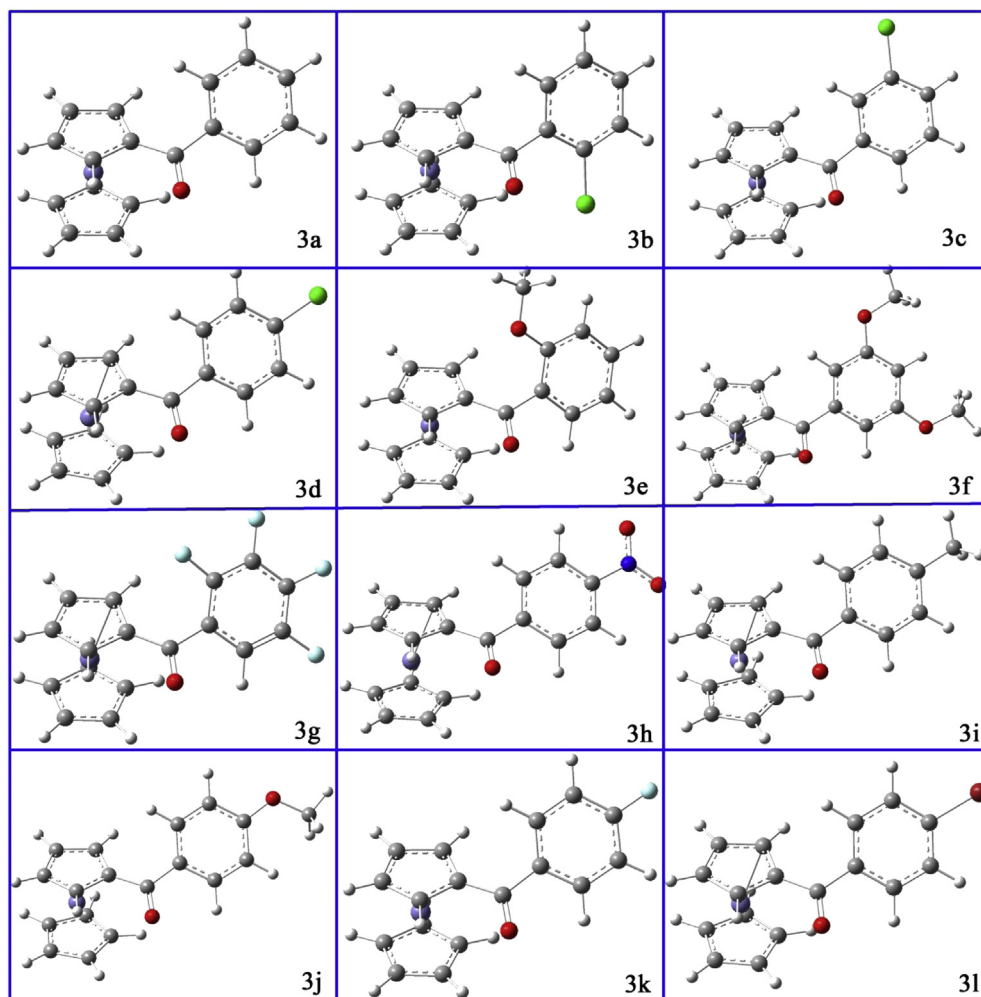


Fig. 6. The geometries optimized by B3LYP/6-31G(d) level.

Table 2
Parts of bond length (in Å) and the dihedral angle (in °) in isomers at B3LYP/6-31G(d) level. The number of C is shown in Fig. 7.

Compound	C ₁ –C ₂	C ₁ –C ₃	C ₁ –O	∠C ₁ –C ₂ –C ₆ –C ₇	∠C ₁ –C ₃ –C ₄ –C ₅
3a	1.485	1.501	1.229	174.4	176.7
3b	1.479	1.511	1.223	174.4	175.7
3c	1.483	1.504	1.228	174.8	176.8
3d	1.483	1.502	1.228	174.3	176.6
3e	1.481	1.506	1.228	173.5	176.6
3f	1.485	1.504	1.228	173.7	177.0
3g	1.475	1.512	1.227	173.5	175.6
3h	1.479	1.507	1.227	174.3	176.3
3i	1.486	1.499	1.229	174.1	176.7
3j	1.487	1.494	1.230	174.2	177.0
3k	1.485	1.499	1.229	174.3	176.6
3l	1.483	1.501	1.229	173.9	176.7

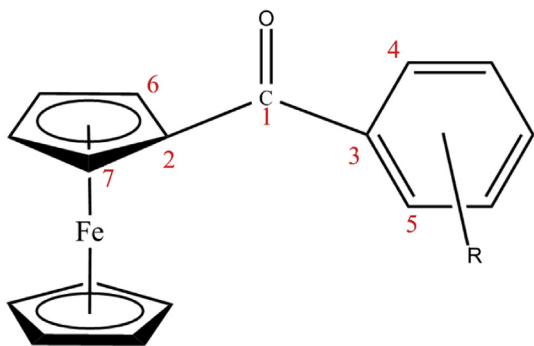


Fig. 7. The structure schematic of carbonyl-type ferrocene. The numbers are construed respectively as the carbon atoms.

through a delay line driven by a stepping motor so that the optical path length difference between the k₂ and k₁ beams could be adjusted during the measurement. The angle between the beams was about 5°. When the beams were overlapped spatially in the sample, the generated signal beam (the phase-conjugated beam k₃) passed through an aperture, which was recorded by a photodiode, and then analyzed by a lock-in amplifier and computer (as shown in Figs. 2 and 3).

2.5. Calculated method

The ground-state geometry of all isomers was optimized at the B3LYP level [25]. And the basis set of 6-31G (d) was used to optimize the geometries. Then the vibrational frequencies were calculated at the B3LYP/6-31G (d) level. The optimized geometries were locating at the local lowest point on the potential energy surface because that all the predicated vibrational spectra had no imaginary frequency [26]. Then the MOs and natural charge analyses at the same level of theory were carried out for some isomers. All the calculations were performed within the Gaussian 09 quantum chemical package [27].

Table 3

The energy (in eV) of the HOMO, LUMO, and HOMO–LUMO gap (E_{HOMO} , E_{LUMO} , E_{gap} in eV) of compounds 3a, 3b, 3e, 3h, and 3i calculated at the B3LYP/6-31G(d) level.

Compound	E_{HOMO}	E_{LUMO}	E_{gap}
3a	–1.500	–5.431	3.930
3b	–1.474	–5.507	4.033
3c	–1.236	–5.303	4.067
3d	–2.770	–5.756	2.986
3e	–1.412	–5.414	4.002

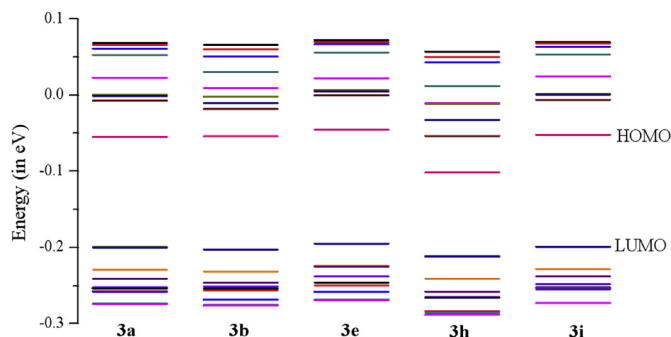


Fig. 8. The energies of the frontier molecular orbitals in the eight isomers at the B3LYP/6-31G(d) level.

3. Results and discussion

Among the 12 benzoylferrocene derivatives, **3f** and **3g** are new compounds. The compounds were synthesized by the Friedel–Crafts reaction from benzenecarbonyl chloride derivatives and ferrocene, as illustrated in Fig. 1.

The linear UV–vis absorption spectra of the 12 benzoylferrocene derivatives in DMF solutions are shown in Fig. 4. These compounds exhibited absorption peaks between 250 and 800 nm. The laser wavelength (800 nm) used in the DFWM experiment was far from their resonant bands. Thus, the third-order NLO susceptibilities $\chi^{(3)}$ of the compounds were off-resonant nonlinear responses.

The third-order NLO susceptibility, $\chi^{(3)}$, is calculated by comparing the measured signal for the sample with that for CS₂ under the same experimental condition. The $\chi^{(3)}$ is obtained according to the following formula [28]:

$$\chi_s^{(3)} = \left(\frac{I_s}{I_r}\right)^{1/2} \frac{L_r (n_s)^2}{L_s (n_r)} \frac{\alpha L \exp(\alpha L/2)}{1 - \exp(-\alpha L)} \chi_r^{(3)}$$

where I is the intensity of the phase-conjugated beam, L is the sample path length, n is the linear refractive index, and α is the linear absorption coefficient. The subscripts 's' and 'r' refer to the sample and CS₂, respectively. The values of $\chi_r^{(3)}$ and n_r for CS₂ are 6.7×10^{-14} esu and 1.632, respectively [29–31].

The temporal response of the phase conjugate signal as a function of the delay time of the input beam is shown in Fig. 5. The response times of the samples could be obtained from this function.

The values of $\chi^{(3)}$, n_2 , γ and response times for the samples deduced and calculated from the experimental results are listed in Table 1.

The benzoylferrocene derivatives **3a**–**3l** possess a highly delocalized π -conjugated electron system. The γ values of the benzoylferrocene derivatives are higher than that of the other third-order NLO materials, such as organobimetallic Ru(II)–Re(I) 4-ethynylpyridyl complexes [32], which is about 6×10^{-34} esu, and are also higher than that of ferrocene, which is 1.6×10^{-35} esu [33].

The fully optimized geometries of the twelve compounds were shown in Fig. 6. The atoms of cyclopentadiene ring (Cp) and the benzene ring (Ph) are all at the plane, respectively. The C of the

Table 4

The Natural charge of some atoms in the compounds 3a, 3b, 3e, 3h, and 3i calculated at the B3LYP/6-31G(d) level. (Unit: e).

	3a	3b	3e	3h	3i
Fe ₂ Cp	0.006	0.023	0.012	0.031	0.006
CO	–0.004	0.026	0.009	0.004	–0.009
R'	0.238(dui)	0.009	–0.195	–0.246	0.039

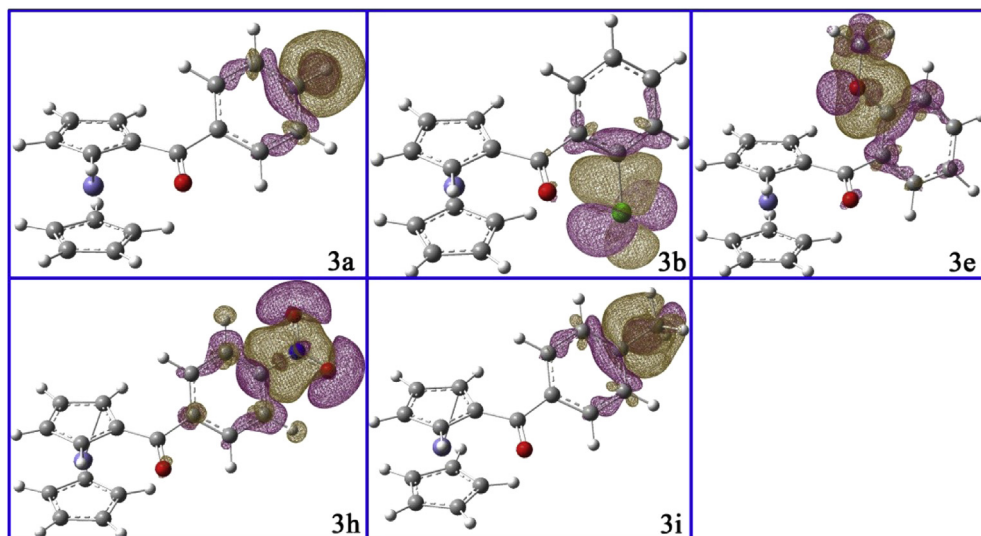


Fig. 9. The charge differential density of the **3a**, **3b**, **3e**, **3h**, and **3i**.

carbonyl group is almost on the Cp plane with the smallest dihedral angle (173.5°) in the compound **3e** and **3g** as shown in Table 2. At the same time, the C of the carbonyl group is almost on the Ph plane with the smallest dihedral angle (175.6°) in the **3g** as shown in

Table 2. The dihedral angle formed by the Cp and Ph is about 45° in all the twelve complexes. And the ferrocene almost unchange the symmetry of D_{2d} in the 12 complexes. The substitutions of $-\text{NO}_2$, $-\text{Cl}$, and $-\text{4F}$ shorten the bond lengths of the C_1 and C_2 (The number

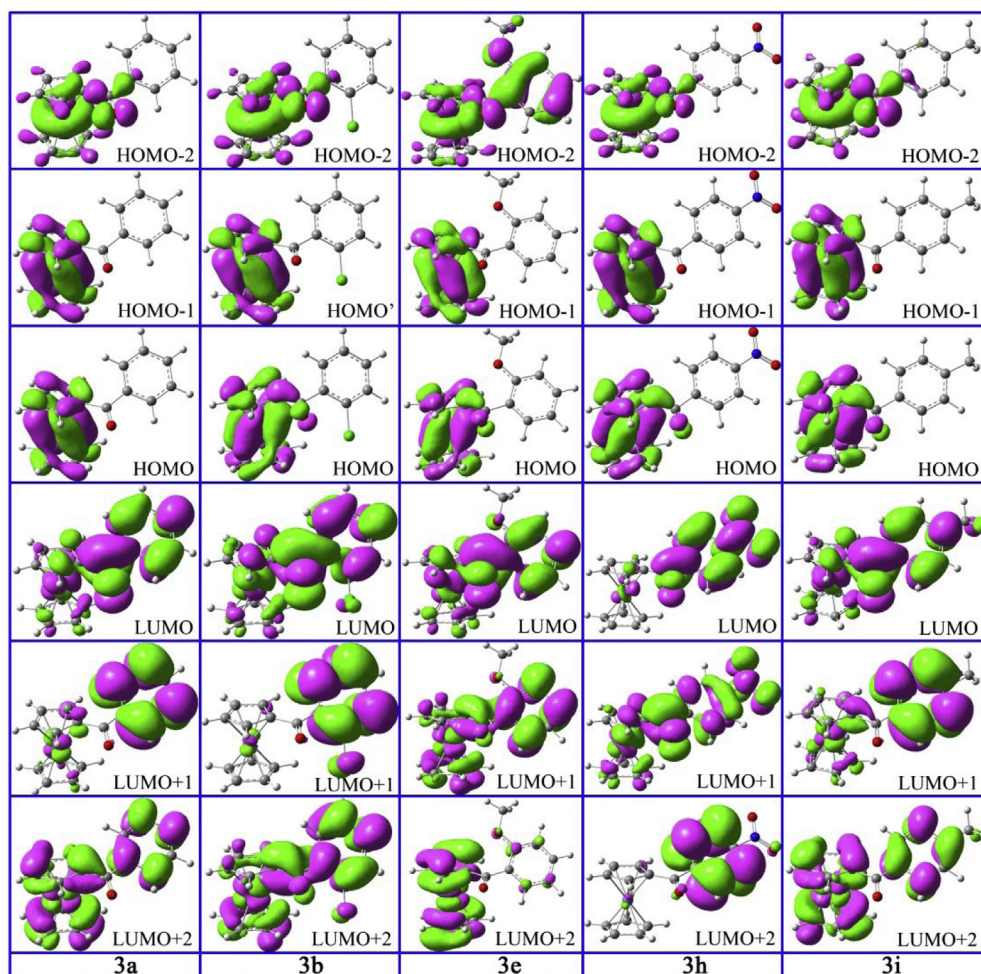


Fig. 10. The frontier molecular orbitals of the **3a**, **3b**, **3e**, **3h**, and **3i**.

of C is shown in Fig 7) and the bond length of C₁–C₃ as shown in Table 3. The electron-withdrawing –NO₂ decreases the energy of HOMO and HOMO–LUMO gap obviously as shown in Table 3 and Fig 8. The lower energy of LUMO illustrates the electron injection was improved. The lower E_{gap} illustrates these compounds with electron-withdrawing substitutional aryl would have larger third-order NLO which accord with the above experiment as well.

These derivatives contain electron-withdrawing substituents aryl radical groups and electron-donating ferrocenyl in the form of a D– π –A structure, resulting in a stronger intermolecular charge transfer. Then the natural charges of some complexes were calculated listed in Table 4. Electron-withdrawing substituents such as the –NO₂ in **3h** has higher natural charge values (–0.246 e) than others as shown in Table 4. And the electron-donating ferrocenyl has the largest natural charge value of 0.031 e in **3h**. The natural charge of the –CO– bridge is very small in all the calculated compounds. The transferred charges to the substituents are accord with the γ values of these compounds in experiment from Table 4. The net charge of –NO₂ in **3h** with –0.246 is much lower than that of –CH₃ with 0.039 in **3i**. The charge differential density (shown in Fig 9) of these five compounds also shown that the –NO₂ has larger effect on the charge density in the **3h** than other compounds. Therefore, the charge transfer to –NO₂ is more than others according with the result from the natural charge. The stronger is the electron-withdrawing ability of the substituents of the aryl groups, the higher are the γ values.

The frontier molecular orbitals (FMOs) of **3a**, **3b**, **3e**, **3h**, and **3i** compounds are listed in Fig. 10. The FMOs (LUMO+2, LUMO+1, LUMO, HOMO, HOMO–1, and HOMO–2) of the five calculated isomers are similar to each other in principal character. The electronic density of HOMO–1 mainly located on the ferrocene, especially the *d* atomic orbital (AO) of Fe atom. The HOMO is similar to the HOMO–1 in every compound. It is worthwhile to refer to that the *p* AOs of C and O of the –CO– bridges had some contributions to the LUMO in the five compounds. The electronic density of LUMO is mainly composed by the *d* AO of Fe, the –CO–, and the Ph in the **3a**, **3b**, **3e**, and **3i**. Different with these compounds, the *d* AO of Fe has small contribution to LUMO in **3h**. This is maybe the main reason why the **3h** with larger third-order polarizability than others.

4. Conclusions

In this study we have described the synthesis, the third-order NLO properties and the DFT study on a serial of benzoylferrocene derivatives possessing D– π –A structures. The third-order NLO properties in the femtosecond range were investigated using the DFWM technique at 800 nm. The third-order NLO susceptibilities of the compounds were $3.065\text{--}7.859 \times 10^{-13}$ esu. The second-order hyperpolarizabilities of the molecules were $1.018\text{--}2.611 \times 10^{-31}$ esu. These compounds possess ultrafast response times of <70 fs. The DFT study showed that the third-order NLO properties were increased with the increasing electron-withdrawing ability in accordance with the decreasing E_{gap} . With the increasing ability of attract electron, the transferred charge to the substituent is increasing, especially in the **3h**. And the affection on the electronic reallocate is increasing with the increasing electron-withdrawing ability.

Acknowledgments

We are very grateful to Dr. Shian Zhang from the Key Laboratory of Optical and Magnetic Resonance Spectroscopy in East China Normal University, for the DFWM experiment and the helpful discussion. This research was financially supported by the National Natural Science Fund of China (Grant no. 20876148).

References

- [1] Wang C, Zhang T, Lin WB. Rational synthesis of noncentrosymmetric metal-organic frameworks for second-order nonlinear optics. *Chem Rev* 2012;112(2):1084–104.
- [2] Hermet P, Fraysse G, Lignie A, Armand P, Papet P. Density functional theory predictions of the nonlinear optical properties in alpha-Quartz-type germanium dioxide. *J Phys Chem C* 2012;116(15):8692–8.
- [3] He N, Chen Y, Bai J, Wang J, Blau WJ, Zhu J. Preparation and optical limiting properties of multiwalled carbon nanotubes with π -conjugated metal-free phthalocyanine moieties. *J Phys Chem C* 2009;113(30):13029–35.
- [4] Ashraf M, Teshome A, Kay AJ, Gainsford GJ, Bhuiyan MDH, Asselberghs I, et al. NLO chromophores containing dihydrobenzothiazolylidene and dihydroquinolylidene donors with an azo linker: synthesis and optical properties. *Dye Pigment* 2013;98(1):82–92.
- [5] Alicante R, Cases R, Forcen P, Oriol L, Villacampa B. Synthesis and nonlinear optical properties of side chain liquid crystalline polymers containing azobenzene push–pull chromophores. *J Polym Sci Polym Chem* 2010;48(1):232–42.
- [6] Li NJ, Lu JM, Li H, Kang ET. Nonlinear optical properties and memory effects of the azo polymers carrying different substituents. *Dye Pigment* 2011;88(1):18–24.
- [7] Ramasamy P, Babu GA. Crystal structure, crystal growth and characterization of novel organic NLO material: 2,4,4'-trimethoxybenzophenone. *Mater Chem Phys* 2010;119(3):533–8.
- [8] Kishida H, Hibino K, Nakamura A, Kato D, Abe J. Third-order nonlinear optical properties of a π -conjugated biradical molecule investigated by third-harmonic generation spectroscopy. *Thin Solid Films* 2010;519(3):1028–30.
- [9] Liu BQ, Sun R, Ge JF, Li NJ, Shi XL, Qiu LH, et al. The synthesis and third-order nonlinear optical properties of resonance benzo a phenoxazinium salts. *Dye Pigment* 2011;88(1):50–6.
- [10] de Baroja NM, Franco S, Garin J, Orduna J, Villacampa B, Borja P, et al. Synthesis, characterization, and optical properties of novel 1,3-dithiole donor-based chromophores. *RSC Adv* 2013;3(9):2953–62.
- [11] Rudresha BJ, Ramachandra Bhat B, Ramakrishna D, Anthony JK, Rotermond F. Third-order optical nonlinear studies of cobalt (II) schiff base complex bearing triphenylphosphine using differential optical kerr gate and Z-scan studies. *Synth Met* 2010;160(13–14):1584–6.
- [12] Yao CB, Zhang YD, Chen DT, Yin HT, Yu CQ, Li J, et al. Study of all-optical switching and optical limiting properties in phenoxy-phthalocyanines liquid. *Opt Laser Technol* 2013;47:228–31.
- [13] Kulhanek J, Bures F, Kuznik W, Kityk IV, Mikysek T, Ruzicka A. Ferrocene-donor and 4,5-dicyanoimidazole-acceptor moieties in charge-transfer chromophores with *p* linkers tailored for second-order nonlinear optics. *Chem Asian J* 2013;8(2):465–75.
- [14] Amer WA, Wang L, Amin AM, Ma LA, Yu HJ. Recent progress in the synthesis and applications of some ferrocene derivatives and ferrocene-based polymers. *J Inorg Organomet Polym Mater* 2010;20(4):605–15.
- [15] Lohan M, Justaud F, Lang H, Lapinte C. Synthesis, spectroelectrochemical, and epr spectroscopic studies of mixed bis(alkynyl)biferrocenes of the type (LnMC)(LnM' C)bfcc. *Organometallics* 2012;31(9):3565–74.
- [16] Keshav K, Singh N, Elias AJ. Synthesis and reactions of ethynylferrocene-derived fluoro- and chlorocyclotriphosphazenes. *Inorg Chem* 2010;49(12):5753–65.
- [17] Jia JH, Tao XM, Li YJ, Sheng WJ, Han L, Gao JR, et al. Synthesis and third-order optical nonlinearities of ferrocenyl schiff base. *Chem Phys Lett* 2011;514(1–3):114–8.
- [18] Jia JH, Dong HQ, Li YJ, Sheng WJ, Gao JR. One-pot process for preparation of ferrocenylethene derivatives via solvent-free Wittig reaction. In: Chen WZ, Li Q, Chen YL, Dai PQ, Jiang ZY, editors. *Adv Mater Res Pts 1–3*, vol. 476–478; 2012. pp. 1218–21.
- [19] Lin XL, Jia JH, Yu WG, Gao JR, Yin Z, ZY F. Synthesis and study of symmetrical schiff base-ferrocene derivative. *Chin J Lasers* 2011;38(10). 1006004-1–4-5.
- [20] Tao XM, Jia JH, Gaoand JR, Zheng YF. Synthesis of amide-containing ferrocenyl organometallic third-order nonlinear optical materials. *J Func Mater* 2011;42(5). 903–906+10.
- [21] Jia J, Cui Y, Li Y, Sheng W, Han L, Gao J. Synthesis, third-order nonlinear optical properties and theoretical analysis of vinylferrocene derivatives. *Dye Pigment* 2013;98(2):273–9.
- [22] Khobragade DA, Mahamulkar SG, Pospisil L, Cisarova I, Rulisek L, Jahn U. Acceptor-substituted ferrocenium salts as strong, single-electron oxidants: synthesis, electrochemistry, theoretical investigations, and initial synthetic application. *Chem Eur J* 2012;18(39):12267–77.
- [23] Wrona-Piotrowicz A, Ceglinski D, Zakrzewski J. Active esters as acylating reagents in the Friedel–Crafts reaction: trifluoromethanesulfonic acid catalyzed acylation of ferrocene and pyrene. *Tetrahedron Lett* 2011;52(41):5270–2.
- [24] Biju AT, Glorius F. Intermolecular N-heterocyclic carbene catalyzed hydroacylation of arynes. *Angew Chem Int Ed* 2010;49(50):9761–4.
- [25] Lee C, Yang W, Parr RG. Development of the colle-Salvetti correlation-energy formula into a functional of the electron density. *Phys Rev B* 1988;37(2):785–9.
- [26] Li W, Wu QF, Ye Y, Luo MD, Hu L, Gu YH, et al. Density functional theory and ab initio studies of geometry, electronic structure and vibrational spectra of

- novel benzothiazole and benzotriazole herbicides. *Spectrochim Acta A* 2004;60(10):2343–54.
- [27] Frisch GWTJ, Schlegel HB, Scuseria GE, Robb MA, Cheeseman JR, Scalmani G, et al. Wallingford CT: Gaussian, Inc.; 2009.
- [28] Pang Y, Samoc M, Prasad PN. 3rd-Order nonlinearity and 2-Photon-Induced molecular-dynamics – femtosecond time-resolved transient absorption, kerr gate, and degenerate 4-wave-mixing studies in poly(para-phenylene vinylene) sol-gel silica film. *J Chem Phys* 1991;94(8):5282–90.
- [29] Orczyk ME, Samoc M, Swiatkiewicz J, Prasad PN. Dynamics of 3rd-Order nonlinearity of canthaxanthin carotenoid by the optically heterodyned phase-tuned femtosecond optical kerr gate. *J Chem Phys* 1993;98(4):2524–33.
- [30] Cai ZB, Gao JR, Li XN. Synthesis and third-order optical nonlinearities of anthracenedione derivatives. *Dye Pigment* 2007;74(2):494–500.
- [31] Jenekhe SA, Chen WC, Lo SK, Flom SR. Large 3rd-order optical nonlinearities in organic polymer superlattices. *Appl Phys Lett* 1990;57(2):126–8.
- [32] Ge Q, Corkery TC, Humphrey MG, Samoc M, Hor TSA. Organobimetallic Ru-II-Re-I 4-ethynylpyridyl complexes: structures and non-linear optical properties. *Dalt Trans* 2009;31:6192–200.
- [33] Ghosal S, Samoc M, Prasad PN, Tufariello JJ. Optical nonlinearities of organo-metallic structures - aryl and vinyl derivatives of ferrocene. *J Phys Chem* 1990;94(7):2847–51.